Available online at www.sciencedirect.com
ScienceDirect
Journal of the Franklin Institute 345 (2008) 640–658
Journal of The Franklin Institute
www.elsevier.com/locate/jfranklin

Characterization of wall dispersive and attenuative effects on UWB radar signals

Ali Muqaibel[a,*], Ahmad Safaai-Jazi[b]

[a]Electrical Engineering Department, King Fahd University of Petroleum & Minerals, P.O. Box 1734, Dhahran 31261, Saudi Arabia
[b]The Bradley Department of Electrical and Computer Engineering, Virginia Polytechnic Institute and State University, Blacksburg, VA 24061-0111, USA

Received 19 September 2007; received in revised form 17 November 2007; accepted 24 January 2008

Abstract

This paper addresses the potentials of ultra-wideband (UWB) through-wall imaging radars compared with conventional narrowband systems. The challenges that limit the utilization of high precision UWB systems are examined with the aim of mitigating them. These challenges include multi-path, pulse dispersion, and antenna effects on the pulse shape due to angles of transmission and arrival. The propagation of UWB signals through walls is a crucial factor in determining the success of UWB radar technology. UWB signals, when propagating through walls, not only suffer attenuation but also distortion due to dispersive properties of the walls. This paper examines time- and frequency-domain techniques for measuring the electromagnetic properties of construction materials in the UWB frequency range. The measured parameters provide valuable insights in appreciating the capabilities and limitations of the UWB technology. Special attention is paid to time gating as a mean to extract the direct-path signal from the multi-path components. Both single-pass and multi-pass models are discussed. Multi-pass models account for the multiple reflections within the wall while the single-pass model assumes the possibility of gating out a single transmission. The partition-dependent narrowband propagation model is modified to account for the ultra-wide bandwidth of the signal. The paper illustrates the application of the modified model in indoor environments. The modified model is helpful in estimating the link power budget. It is also useful in studying the performance of UWB systems for indoor communication and positioning applications.

Keywords: Ultra-Wideband (UWB); Trough-wall; Dispersion; Propagation; Rader; Impulse radio; Insertion loss

*Corresponding author. Tel.: +966 3 8601595; fax: +966 3 8603535.
E-mail address: muqaibel@kfupm.edu.sa (A. Muqaibel).

0016-0032/$32.00
doi:10.1016/j.jfranklin.2008.01.002

1. Introduction

Ultra-wideband (UWB) communication systems are generally defined as systems, which exhibit a transient impulse response. A UWB transmitter is defined as an intentional radiator that, at any point in time, has a fractional bandwidth of greater than or equal to 0.2 or occupy a bandwidth greater than 500 MHz regardless of the fractional bandwidth [1]. UWB radars are attracting increasingly more interest after the proposal by Scholtz [2] to use impulse UWB radio for personal wireless communication applications. UWB technology supports the integration of communication and radar applications such as imaging and positioning [3–5].

Time-modulated UWB signals are superior to narrowband signals by providing orders of magnitude improvement in spatial resolution. This could result in sub-centimeter range resolution. There are many situations where UWB high resolution signals can be utilized. For example, UWB technology can be used to augment the global positioning satellite system (GPS). UWB signals are immune to multi-path distortions, which are a major problem for indoor narrowband receivers. If reference stations are equipped with UWB technology, precise locations can be determined especially within buildings and areas where GPS fails to operate. This technology also allows aircraft to determine and monitor their position relative to other aircrafts and relative to the ground. Another promising application of the UWB technology is in automobile collision avoidance, and newer and more sophisticated applications are expected to emerge due to recent developments in this rapidly evolving technology.

UWB systems are anticipated to offer better wall-penetration capabilities. UWB through-wall imaging systems are allocated a bandwidth below 960 MHz or between 3.1 and 10.6 GHz. These systems detect the location or movement of persons or objects located on the other side of the wall. The technology is being tested to look inside closed rooms. Narrowband technology relies on high frequency (short wavelength) radio waves to achieve high resolution. However, shortwave signals cannot penetrate effectively through materials, while UWB radars promise good penetration through materials and has time resolution to within a fraction of nanosecond.

Recent years have witnessed increasing research activities devoted to the UWB through-wall technology. Attiya et al. [6] experimentally studied the potentials and limitations of through-wall human body detection by means of UWB signals. They concluded that the loss and dispersive properties of the wall cause a low-pass filtering effect, which limits the high resolution capability of the original UWB pulses. Mahfouz et al. [7] developed a compact UWB radar for see-through-walls applications. The image is formed by scanning a beam across the radar scene and utilizing a receiving array and beam-forming process. Chia et al. [8] developed a UWB radar for medical imaging that can measure the heartbeats and breathing rate of human in a 1-m range. The system was also successfully tested with a targeted human object obstructed with a typical wall partition. Regarding the impact of wall and obstructions on UWB indoor ranging, it is reported in [9] that the average ranging error for line-of-sight (LOS) scenarios is 6 cm. This error increased to 24, 38, and 84 cm for sheet rock, plaster, and cinder block wall materials, respectively, in none-LOS (NLOS) conditions. Hantscher et al. [10] has described a complete low-cost UWB radar system for wall scanning applications. The proposed system can reconstruct the shape of simple targets like water pipes.

The propagation of UWB signals through walls is an important issue with direct impact on the extent of future successes of UWB radar technology. The propagation of UWB signals, as an electromagnetic wave, is governed, among other things, by the properties of materials in the propagation medium. The information on electromagnetic properties of building materials in the UWB frequency range provides valuable insight in understanding the capabilities and limitations of UWB technology for indoor and indoor–outdoor applications.

Many researchers have studied the propagation of electromagnetic waves through walls. For example, Hashemi [11] reviewed and summarized much of the earlier investigations on electromagnetic characterization of building materials. During recent years, many more investigations on evaluating electrical properties of various building materials over different frequency ranges have been carried out. Typical materials examined include concrete, plasterboard walls, limestone concrete blocks, glass, bricks, cement-based materials, and wood. The information in the literature is presented in terms of penetration loss, dielectric constant, loss tangent, permittivity, conductivity, and reflection and transmission coefficients [12–19]. Extensive data on dielectric properties of a variety of glasses [20], wood and wood-based materials, but mainly at frequencies outside the UWB range, have also been reported [21].

It is noted from the cited work that the available information on building material properties are largely over narrowband frequencies and often limited to few materials. UWB signals not only suffer attenuation as in the case of narrowband signals when propagate through walls, but also suffer distortion due to dispersive properties of the walls. In narrowband measurements, only the attenuation represented by the magnitude of insertion transfer function (i.e. insertion loss) has been the quantity of interest. However, for UWB signals in addition to the magnitude, dispersion is an essential factor that needs to be accounted for in studying the propagation effects. Therefore, existing through-wall measurements and models, although helpful in providing some general understanding, are not adequate for UWB imaging applications.

The objective of this paper is to examine the potentials of UWB through-wall imaging and UWB radars. The impacts on wall penetration, including attenuative and dispersive effects, will be examined. The paper starts by discussing the challenges faced by UWB imaging devices including multi-path, multiple reflections inside the wall, and power loss. To characterize the impacts on through-wall propagation, both time-domain and frequency-domain measurement setups and procedures are discussed. The mathematical models that link the measured data with the representative parameters are presented next. The difference between single pass and multiple pass are then explained. The results of this investigation provide valuable insights into the transient behavior of short pulses as they propagate through typical walls and structures. A partition-dependent narrowband model is modified to account for the frequency variation within the UWB range of frequencies. The paper concludes with remarks on the future of UWB imaging.

2. UWB through-wall imaging challenges

As UWB signals propagate through walls, they suffer degradation due to both attenuation and dispersion. Material absorption, multiple reflections, and frequency dependence of the dielectric constant of materials are the main contributors to these signal degrading effects. To achieve the high resolution offered by UWB systems, one has to

develop advanced decision-making and signal processing techniques that mitigate propagation impairments occurring in the medium between the transmitter and the receiver. Multi-path, obstructions, and antenna effects are among the challenges that should be dealt with.

The first challenge is the multi-path reception. In general, UWB signals are very immune to multi-path. However, there are cases where the transmitter and/or the receiver are very close to a wall or a table that causes pulses from different multi-path components to overlap and reduce the timing and positioning capability of the system.

The second challenge is caused by the multiple reflections within the wall. This impact becomes more dominant if the wall is heterogeneous. The dielectric constant of the obstructions and their thickness introduce variable delay in the propagation path. The travel time through the thickness of the objects in the signal path is critical to the delay measurement when high accuracy is desired. To illustrate the effect on the delay, amplitude and pulse shape, different materials are inserted in the path between transmit and the receive antennas. First, a free-space measurement is conducted, then a slab of material is inserted and the through signal is acquired. Here two examples are presented to illustrate the effect of the obstruction material on the signal delay and hence positioning capability. For additional examples the reader is referred to [18]. In the first example, a typical plywood as a relatively homogeneous material is used. The thickness of the plywood is 1.52 cm. The second example is for typical construction concrete blocks with air holes. The thickness of the wall made of concrete block is 19.45 cm. Fig. 1 illustrates the free-space and through measurements for the two cases. The generated pulse is a Gaussian-like waveform with a full-width half-maximum (FWHM) of 85 ps. Due to the impact of the antenna, the received signal has a shape, which is the derivative of Gaussian pulse. The damped ringing effects result in the second peak, which can be noted in the figure.

The third challenge is imposed by the high power loss which is a result of thick walls or very lossy material like reinforced concrete. Weak signal levels cannot be measured accurately due to presence of noise and limited dynamic range of measurement equipment.

Another important challenge is associated with UWB antennas. In practical cases, the radiation pattern, input impedance, and polarization of the antenna play an important role. The difficulty when using omni-directional antennas, which can cause stronger multi-path, is more pronounced than the case of directional antennas. To illustrate this effect, which in essence is due to the angle of arrival, different experiments and scenarios are considered.

One scenario is to investigate the effect of vertical rotation of an antenna (E-plane scan). In this case, the transmit antenna is kept at a fixed height and position and the receive antenna, while kept at a fixed height, is rotated along the elevation angle, θ. Measurements are performed at the angles $\pm 15^\circ$, $\pm 30^\circ$, $\pm 45^\circ$, $\pm 60^\circ$. The schematic diagram embedded in Fig. 2a illustrates the first two multi-path components that are captured by the receive antenna. Circular lines covering the receiver represent the rotation in the vertical direction as well as the antenna far-distance electric field lines. Negative angles refer to rotation towards floor, while positive angles represent rotation in the reverse direction. When the receive antenna is tilted more towards the floor, i.e. negative angles, the LOS pulse and the reflection off the floor tend to move towards each other and vice versa. A more interesting feature is the broadening of the original pulse when compared directly to the boresight reception. The effect of horizontal rotation of the antenna (H-plane scan) is depicted in Fig. 2b. Positive and negative angles refer to left and right rotations, respectively. In view

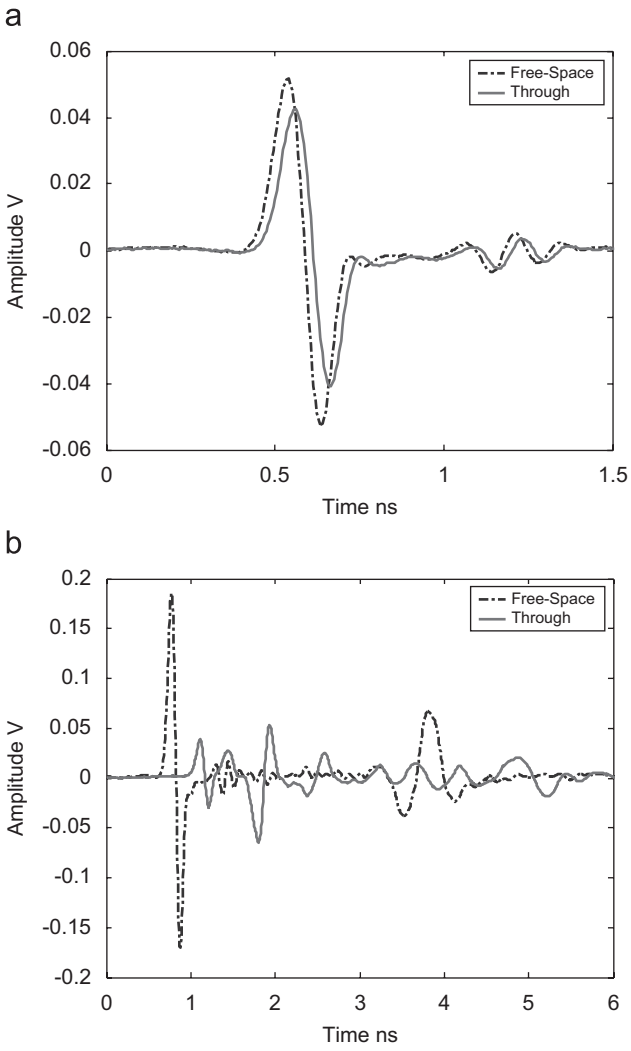

Fig. 1. 'Free-space' and 'through' measurements to illustrate delay and pulse deformation: (a) plywood and (b) concrete blocks.

of Fig. 2b, rotation in either right or left direction produces identical results. That is because the left and the right rotations are symmetrical about the boresight direction. An important feature is the swift broadening of the original pulse when compared directly to the boresight reception. A more comprehensive characterization can be done in anechoic chamber. Typically, antenna characterization is preformed in the frequency domain for only specific frequencies. For accurate time domain applications, such task requires a huge number of frequency measurements [22].

These challenges and finding ways of effectively dealing with them call for accurate measurement and characterization of UWB through-wall propagation. The next two sections address the techniques for measuring and modeling the attenuative and dispersive properties of through-wall propagation.

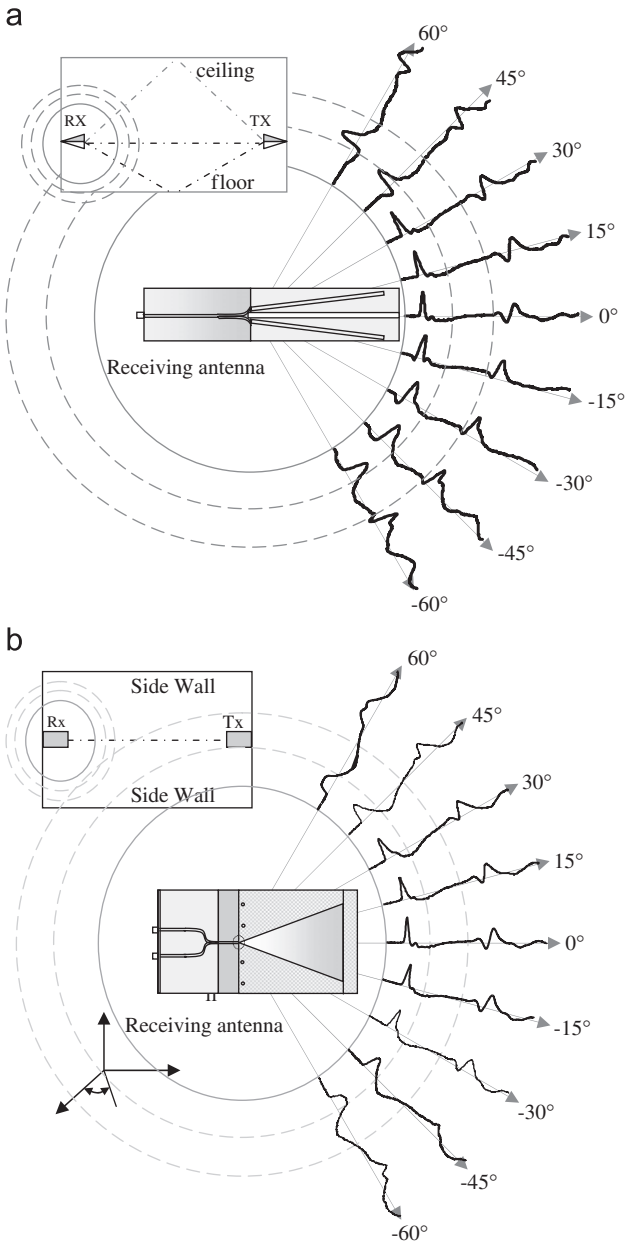

Fig. 2. Received waveforms at different angles: (a) different elevation angles and (b) different azimuth angles.

3. Techniques for measurement of attenuation and dispersion through walls

Unlike narrowband wireless communication systems in which signal distortion is essentially caused by multi-path components, in UWB communication systems the information signal may suffer significant distortions due to dispersive properties of wall

materials in the propagation path, multi-path components, and also bandwidth limitations of transmit and receive antennas. In this section, techniques for measurement of attenuation and dispersion of UWB pulses propagating through walls are discussed. In particular, time-domain as well as frequency-domain radiated measurement techniques, which lend themselves to nondestructive and in situ applications, are addressed.

3.1. Time-domain technique

In the time-domain technique, a periodic train of very short-duration Gaussian-like pulses separated by sufficiently long quiet intervals is used for measurement of UWB signal propagation. These pulses are radiated by means of a UWB antenna with sufficiently large bandwidth to cause negligible signal distortions. On the receiving end, the signal is captured by another UWB antenna and detected by means of a wideband detector such as a digital sampling oscilloscope. The measurement setup, as shown in Fig. 3, consists of a pair of transmit and receive UWB antennas such as TEM horns, a pulse generator, a digital sampling oscilloscope, and a triggering signal generator. The pulse generator is connected to the transmit antenna through a low-loss wideband cable followed by a balun which converts the unbalanced coaxial cable terminals to the balanced antenna feed terminals. When higher amounts of radiated power are needed, a UWB power amplifier may be used at the feed point of the transmit antenna. The receive antenna followed by a balun is connected to the digital sampling oscilloscope by means of a wideband coaxial cable. To increase the received signal power, a low-noise amplifier may be used at the output terminals of the balun. The amplifiers and baluns each should have a constant gain and a linear phase characteristic over the spectrum of the UWB pulse.

Synchronization of both transmit and receive sides of the propagation channel is an important requirement in time-domain measurements. To maintain synchronization, a low-jitter triggering signal is established between the pulse generator and the digital sampling oscilloscope. The sampling oscilloscope requires a pre-trigger. This is achieved by using a step generator driver that can supply the required trigger and pre-trigger signals.

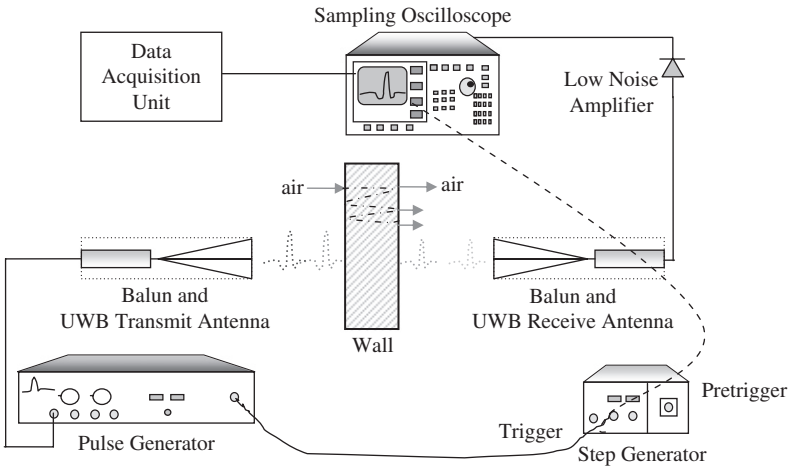

Fig. 3. Schematic of setup for time-domain measurements.

The time delay introduced by the triggering cables and the propagation path of the pulse is compensated by adjusting the time delay between the pre-trigger and the delayed trigger signals. Calibration and noise are two other important issues which need to be addressed. The purpose of calibration is to eliminate the effects of nonideal characteristics of measurement instruments from the measured data. Also, received UWB signals may suffer degradation due to interference and noise from various sources. The narrowband noise is usually due to electromagnetic interference from nearby narrowband systems and often takes the form of a sinusoidal waveform added to the received signal. This type of noise can be eliminated through bandpass filtering. The wideband noise, on the other hand, is typically in the form of random short pulses and can be significantly reduced through multiple signal averaging, a feature generally available in sampling oscilloscopes.

UWB characterization of attenuation and dispersion that a pulse suffers upon propagation through walls is performed based on the measurement of an insertion transfer function defined as the ratio of Fourier transforms of two signals—the received pulse passing through the wall and the signal propagating through free space used as a reference. The complex dielectric constant of the wall material can then be extracted from the insertion transfer function as discussed in the next section. The real and imaginary parts of the dielectric constant account for delay distortions and attenuation suffered by the UWB pulse.

3.2. Frequency-domain technique

In the frequency-domain technique, through-wall propagation measurements are performed at different frequencies using a sweep harmonic generator. The chief advantage of the frequency-domain technique over the time-domain method is that it provides a much larger dynamic range. Each measured data point is represented by a complex number expressed by its magnitude and phase terms. Fig. 4 illustrates the frequency-domain measurement setup. A network analyzer is used for performing sweep frequency measurements. As shown in this figure, port 1 of the S-parameter test set is connected to the transmitter while its port 2 is connected to the receiver. The network analyzer sweeps the frequency within the measurement band of interest. For UWB characterization, because of the ultra-wide frequency range that needs to be swept, one has to make a trade off between the frequency resolution and the required number of measurements that is directly proportional to the time it takes to perform the experiment as well as data storage requirements.

Channel measurements involving long propagation distances require long cables to connect the S-parameter test set ports to the transmitter and/or receiver. Such long cables pose a major limitation, because at high frequencies cable losses increase exponentially, causing significant reduction in the dynamic range. To overcome this problem, one may replace the cable connecting port 1 to the transmitter with a fiber-optic transmission system while using a short coaxial cable connecting the receiver to port 2. The advantages of using optical fibers are very low-transmission loss compared with traditional coaxial cables and immunity to electromagnetic interference; however, fiber-optic systems are much more expensive.

Complex transfer function measurements, expressed in terms of magnitude and phase, are performed using a vector network analyzer (VNA). However, direct phase measurements in UWB communication channels involving long propagation distances

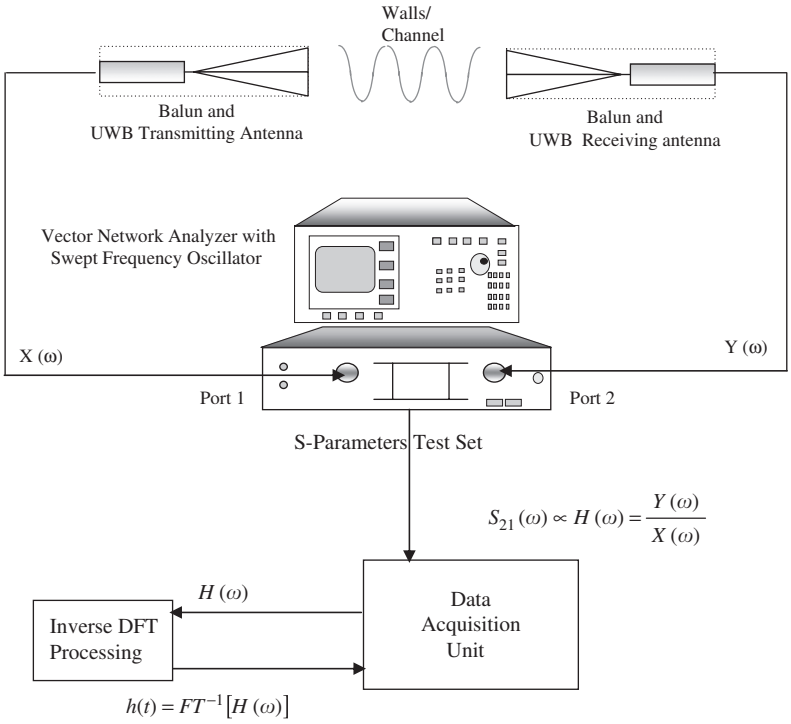

Fig. 4. Frequency-domain measurement setup.

should be dealt with very carefully, as the available VNAs are generally designed for the measurement of complex S-parameters of small two port networks rather than characterization of communication channels with long propagation distances. Errors in direct phase measurements occur due to the difference between the measured frequency and the frequency of the received signal caused by the propagation delay time through the channel. In the sweep mode operation, the VNA frequency changes linearly with the sweep time. With long propagation paths, the frequency of the signal at the end of the channel would be different from that at the beginning, resulting in errors in both magnitude and phase measurements. To avoid sweep mode errors, frequency stepping instead of frequency sweeping may be used. In the frequency stepping mode of operation, the time of the frequency step should be larger than the time delay between transmit and receive antennas. It is emphasized that the measured signal is the one recorded at the end of the step rather than the average of measured signals received during the time step.

Alternatively, frequency-domain measurements may be carried out using a scalar network analyzer that costs much less than a VNA. In the scalar frequency-domain method, only the magnitude of the transfer function can be measured. However, both magnitude and phase information are needed for complete characterization of wall attenuation and dispersion. Under certain conditions, the phase information can be retrieved from the magnitude data by means of a Hilbert transform technique. The required conditions are that the impulse response of the UWB channel should be causal and analytic. That is, the received signal does not arrive sooner than the corresponding

free-space delay time, and for a finite energy pulse, the amplitude of the pulse decays to zero after a reasonable amount of time. Furthermore, the amplitude of each multi-path component should be smaller than that of the one preceding it. These requirements are satisfied for through-wall propagation and generally for most LOS scenarios. It is known that for a causal analytic signal, the imaginary part of its Fourier transform is equal to the Hilbert transform of the real part. Accordingly, the complex spectrum of a causal analytic signal can be expressed in terms of its magnitude as [23]

$$R(\omega) = |R(\omega)| \exp[\mathrm{j}\mathscr{H}(\ln(|R(\omega)|))], \tag{1}$$

where $\mathscr{H}(\cdot)$ denotes Hilbert transform.

4. Through-wall propagation models

In order to assess the attenuation and dispersion of a signal when propagating through a wall, the complex dielectric constant of the wall need to be determined. This can be accomplished in two steps: (i) measuring the insertion transfer function using the time-domain or frequency-domain technique discussed in the previous section and (ii) developing a mathematical expression which relates the insertion transfer function to the complex dielectric constant of the wall material. The insertion transfer function, denoted as $H(\omega)$, is obtained from the ratio of two signals as defined below:

$$H(\omega) = \frac{V(\omega)}{V^{\mathrm{fs}}(\omega)} = \frac{FT\{v(t)\}}{FT\{v^{\mathrm{fs}}(t)\}}, \tag{2}$$

where $v^{\mathrm{fs}}(t)$ and $V^{\mathrm{fs}}(\omega)$ are reference time-domain and frequency-domain signals, respectively, measured in the absence of the wall (that is, when the wall is replaced with free space), while $v(t)$ and $V(\omega)$ are the time-domain and frequency-domain signals measured in the presence of the wall. In Eq. (2), FT denotes Fourier transform that is used to convert the measured time-domain signals to the frequency domain.

In performing the measurements, transmit and receive antennas are kept at fixed locations and aligned for maximum signal reception. The wall is placed at nearly the mid-point between the two antennas. The distance between transmit and receive antennas should be sufficiently large such that the wall is in the far field of each antenna. This ensures that the radiated field incident on the wall is essentially a plane wave. Thus, propagation through the wall may be modeled as a uniform plane-wave incident upon a lossy dielectric slab of thickness d and complex relative permittivity $\varepsilon_{\mathrm{r}} = \varepsilon'_{\mathrm{r}} - \mathrm{j}\varepsilon''_{\mathrm{r}}$. It is also assumed that the wall and antennas are aligned such that the plane wave is normally incident on the wall. This is a simple electromagnetic problem that can be easily solved. The incident plane-wave establishes a reflected wave in the region where the transmit antenna is placed, a set of forward and backward traveling waves inside the wall, and a transmitted wave in the region where the receive antenna is located. Writing the electric and magnetic field expressions in the three regions and imposing the boundary conditions at the slab–air interfaces, the transmission coefficient T and then the insertion transfer function $H(\omega) = T\mathrm{e}^{\mathrm{j}\beta_0 d}$ are readily obtained:

$$H(\omega) = \frac{4\mathrm{e}^{\mathrm{j}\beta_0 d}}{\mathrm{e}^{\gamma d}(2 + (\eta_0/\eta) + (\eta/\eta_0)) + \mathrm{e}^{-\gamma d}(2 - (\eta_0/\eta) - (\eta/\eta_0))}, \tag{3}$$

where $\beta_0 = \omega\sqrt{\mu_0\varepsilon_0}$, $\gamma = \alpha + \mathrm{j}\beta = \mathrm{j}\omega\sqrt{\mu_0\varepsilon_0(\varepsilon'_{\mathrm{r}} - \mathrm{j}\varepsilon''_{\mathrm{r}})}$, $\eta_0 = \sqrt{\mu_0/\varepsilon_0}$, and $\eta = \eta_0/\sqrt{\varepsilon'_{\mathrm{r}} - \mathrm{j}\varepsilon''}$.

With the insertion transfer function, $H(\omega)$, determined from Eq. (2) by measurements, Eq. (3) can be solved numerically for the complex dielectric constant $\varepsilon_r = \varepsilon'_r - j\varepsilon''_r$. It should be noted that (3) is a complex equation and its numerical solution requires a two-dimensional root search technique.

If the wall material is low loss, $\varepsilon''_r/\varepsilon'_r \ll 1$, allowing considerable simplifications to be made, and ε_r and ε''_r be obtained from separate real expressions. The benefit of the simplified solution is that instead of time consuming two-dimensional root search only one-dimensional root search needs to be implemented. The details of the simplified analysis are available in [24]. Here, a summary of results are presented. The real part of the dielectric constant, ε_r, can be calculated by solving the following equation:

$$\tan[\beta_0 d - \angle H(\omega)] + \frac{1 - QX}{1 + QX}\tan(\beta d) = 0, \tag{4}$$

where $\beta = \beta_0\sqrt{\varepsilon'_r}$, $Q = -[(\sqrt{\varepsilon'_r} - 1)/(\sqrt{\varepsilon'_r} + 1)]^2$, and

$$X = amp;\left\{\left[\cos(2\beta d)(\varepsilon'_r - 1)^2 + 8\varepsilon'_r/|H(\omega)|^2 \right.\right.$$
$$\left.\left. amp;-\sqrt{\left[\cos(2\beta d)(\varepsilon'_r - 1)^2 + 8\varepsilon'_r/|H(\omega)|^2\right]^2 - (\varepsilon'_r - 1)^4}\right]\right\}/\left(\sqrt{\varepsilon'_r} - 1\right)^4.$$

After ε_r has been determined, the imaginary part of the dielectric constant, ε''_r, is obtained from

$$\varepsilon''_r = \frac{c\sqrt{\varepsilon'_r}\ln(X)}{\omega d}, \tag{5}$$

where c is the velocity of light in free space.

An estimate of the average dielectric constant could also be obtained through peak-to-peak impulse time delay, $\Delta\tau$. An average value of the dielectric constant that does not contain the frequency dependence is given by

$$\varepsilon'_r \cong \left[1 + \frac{\Delta\tau}{d/c}\right]^2. \tag{6}$$

5. Structural properties and time gating

A plane wave incident on a wall, as depicted in Fig. 3, establishes a reflected wave in region I (air), a set of forward and backward traveling waves in region II (material), and a transmitted wave in region III (air). Using the boundary conditions for the electric and the magnetic fields at the wall–air interfaces, the transmission coefficient can be calculated using the model presented in Section 4. With this model a multi-pass transfer function is obtained which accounts for all the transmitted waves including the ones resulting from multiple reflections within the wall.

Time gating can also be used to isolate a desired portion of the received signal, namely, the first pass of the pulse signal transmitted through the wall. In this application, the thickness should be large enough to yield sufficient delay. Thus, not only zooming on and extracting the first-pass pulse, but also removing multi-path components and all delayed pulses due to multiple reflections inside the wall becomes possible.

The free-space and through-wall measurements would be most accurate if performed inside an anechoic chamber, which absorbs all multi-path components and reflections from the floor and ceiling. Ideally, to avoid scattering from the edges, the sample slab to be measured should be infinitely wide. Also, samples under test have to be in the far-field regions of transmit and receive antennas, typically several meters for the frequency range of interest and dimensions of the antennas used. Maintaining these requirements is not a convenient task, keeping in mind that absorbers and chamber environment do not allow easy movements of large samples. Fortunately, time gating can be used to reduce significantly the undesired effects such as scattering from edges and reflections from the surrounding walls. For time gating to be efficiently implemented, three conditions have to be met. First, the transmit and the receive antennas should be positioned away from the reflecting surfaces. Second, samples should have relatively large surface dimensions in order to minimize the edge effects. Finally, there should be flexibility in adjusting the distance between the antenna and the sample.

Time gating is required to remove multi-path components from the received signal resulting from surrounding walls and scattered fields from sample edges, as they are not accounted for in-calculation and extraction of material parameters in a single-pass model. The same technique can be used to eliminate antenna ringing and other extraneous effects. However, perfect time gating cannot be achieved because, strictly speaking, infinite acquisition time is required to capture all multiple reflections from the wall interior, and the boresight signal might have small overlaps with multi-path components and scattered fields from the sample edges. Fortunately, because higher-order multiple reflections die out quickly for materials of interest, time gating capabilities are enhanced with shorter pulse durations and larger distances between the test material and reflectors and/or scatterers. If single pass is desired, pulse duration should be shorter than twice the travel time through the slab thickness in order to avoid pulse overlapping.

The choice of the analysis technique is based on how satisfactorily time gating can be implemented. In many cases, multiple reflections inside the slab decay rapidly so that single-pass and multiple-pass techniques essentially yield the same results. If single pass is desired, the previous model should be modified accordingly.

5.1. Single-pass technique

Single-pass technique can be used if the duration of the pulse is sufficiently short or the thickness of the wall or material slab under test is large enough to allow eliminating, by means of time gating, the portions of the signal due to multiple reflections inside the slab which are delayed more than the pulse width. The derivations pertaining to the short-pulse propagation measurements are available in [25]. The results are summarized below:

$$\varepsilon_r(f) \cong \left[1+\frac{\Delta\tau(f)}{\tau_0}\right]^2 = \left[1-\frac{1}{2\pi\tau_0}\frac{d\Phi_{sp}(f)}{df}\right]^2, \tag{7}$$

$$p_e(f) \cong -\frac{1}{\pi f\tau_0\sqrt{\varepsilon_r(f)}}\ln\left[\frac{[1+\sqrt{\varepsilon_r(f)}]^2}{4\sqrt{\varepsilon_r(f)}}|H_{sp}(f)|\right], \tag{8}$$

where $H_{sp}(f) = |H_{sp}(f)|\exp[j\Phi_{sp}(f)]$ is the single-pass insertion transfer function. It is the ratio of the Fourier transform of the single-pass received signal when the slab is in place to

the Fourier transform of the single-pass received signal in the absence of slab. Assuming a fictitious layer of free-space of the same thickness as the material slab, the propagation through this layer involves simply a delay equal to $\tau_0 = d/c$, where d is the layer thickness and c is the speed of light in free space. It should be noted that the derivative term $\mathrm{d}\Phi_{\mathrm{sp}}(f)/\mathrm{d}f$ in Eq. (7) is based on the assumption that the phase varies linearly with frequency. The advantage of using the derivative of the phase is to avoid tracking the unwrapped phase function. As a function of the unwrapped phase, the dielectric constant is given by

$$\varepsilon_{\mathrm{r}}(f) \cong \left[1 + \frac{\Delta\tau(f)}{\tau_0}\right]^2 = \left[1 - \frac{\Phi_{\mathrm{sp}}(f)}{2\pi\tau_0 f}\right]^2. \tag{9}$$

5.2. Multiple-pass technique

If the single-pass signal cannot be gated out satisfactorily, multiple reflections from the slab interior that constitute part of the received signal must be considered. This situation particularly arises when the transit time through the thickness of the slab is small compared to the pulse duration. In this case, an insertion transfer function that accounts for multiple reflections of a homogenous wall is needed. The model presented in Section 4 can be used to determine the complex dielectric constant from the measured insertion transfer function.

To appreciate the difference between the single-pass and multi-pass formulations, the results for the dielectric constant obtained from the two sets of solutions mentioned above are depicted in Fig. 5. It is noted that the results from two solutions are in excellent agreement for the case of plywood. This agreement is due to the fact that for this specific sample (plywood), multiple reflections inside the wood are very small compared to the first single pass. This is not true for glass with a thickness of 0.236 cm. Single-pass assumption is not appropriate for glass because, even with time gating, single pass cannot be accurately obtained. At high frequencies the wavelength is smaller and the assumption of thick wall becomes more reasonable. The thickness of the slab or wall to be characterized is a critical parameter. If the thickness is very small, errors become more pronounced. For example, to estimate the dielectric constant of a slab of glass with 0.236 cm thickness, one should be able to measure the delay occurring when the incident signal permeates this thin layer. If the thickness is larger, there will be longer delays to measure and hence less error will occur. On the other hand, very thick slabs may cause high losses, resulting in weak received signal levels that cannot be accurately measured.

Indoor building materials can be classified into two groups: homogeneous with uniform structures like drywall, wooden doors, plywood, and glass and heterogeneous with nonuniform structures like brick, concrete block, and office partition. The previous analysis assumes a uniform and homogeneous slab or wall. If the measured sample is nonhomogeneous the extracted parameters will be the effective parameters of an equivalent uniform slab. The wall and its equivalent yield the same transmitted fields $(\vec{E}^{\mathrm{t}}, \vec{H}^{\mathrm{t}})$ for the same incident fields $(\vec{E}^{\mathrm{i}}, \vec{H}^{\mathrm{i}})$.

The dielectric constant of materials with uniform structures generally tends to decrease with frequency, whereas the dielectric constant of the material with nonuniform structures exhibits a more complex behavior [18]. Particular behaviors in the loss tangent of such

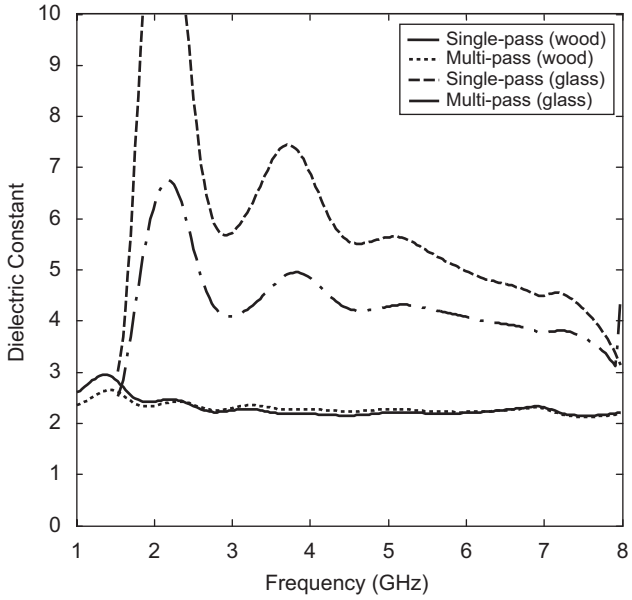

Fig. 5. Comparison of different measurement and analysis techniques.

materials are also observed. For example, the dielectric constant of brick increases with frequency and the loss tangent of concrete block seems to exhibit a resonant behavior at several frequencies. The differences in the behavior may be attributed to the fact that, in addition to material properties, their internal structural characteristics also influence the effective dielectric constant.

Results of the dielectric constant and loss tangent versus frequency for different materials are available in Ref. [18]. Comparing the results obtained by different researchers, clearly indicate that the results for the dielectric constant of materials tested are sufficiently accurate. Variations in the composition of materials used by different researchers result in minor discrepancies in the measured parameters. For most materials, measuring the loss is a more difficult task than measuring the real part of the complex relative permittivity. In many cases, the insertion loss of a wall is largely due to the reflection and much less due to the absorption of the signal, thus the inaccuracies in loss tangent do not have a major impact on pathloss evaluations.

In the following section, we propose a frequency-dependent model for the propagation of UWB signals through walls. The model utilizes the measured parameters to perform simulations.

6. UWB frequency-dependent partition propagation model

When propagating through walls, UWB signals suffer more severe degradations than narrowband signals, because of the effects of frequency-dependent dielectric constants of wall materials in the propagation paths. In narrowband signals, the entire spectrum travels with same speed and suffers the same attenuation, thus no material dispersion effect. On the other hand, in UWB cases, each spectral component of the signal undergoes a different

amount of delay and suffers a different amount of attenuation, because the complex dielectric constant varies with frequency. In fact, this has been the prime motivation for the UWB characterization of building materials presented earlier.

In order to appreciate the significance of signal distortion in UWB applications, let us first examine the propagation of a short bipolar Gaussian pulse through different walls. This problem can be treated using the transmission-line method in conjunction with the Fourier and inverse Fourier transforms. The waves incident on and refracted from the wall are assumed to be plane waves. The effects of transmit and receive antennas are not included in the simulation. The distance between the wall and either antenna is assumed to be large enough such that the plane-wave assumption holds.

Large-scale path losses can be modeled assuming logarithmic attenuation with various types of structures between transmit and receive antennas [11]. Adding all individual attenuations measured in dB yields the total dB loss [11]. Furthermore, it is important to note that when assuming no dispersion takes place, a narrowband approximation is implied. This assumption is not as good for UWB because the magnitude of the transfer function decreases slowly with frequency. The phase is not perfectly linear but here we concentrate on the magnitude impact.

Many results for propagation through walls have been published. However, these results were often obtained at specific frequencies. For UWB characterization, one has to define the pulse shape or its spectrum. It is emphasized that results generated for a specific pulse shape might not be generalized to other UWB signals.

The remaining part of this section introduces a frequency-dependent partition model. A detailed example is presented to illustrate the use of the model. The results for the loss of tested materials presented in [18] are used to develop the frequency-dependent through-wall propagation model. The partition based penetration loss is defined as the path-loss difference between two locations on the opposite sides of a wall [26]. The penetration loss is equal to the insertion loss. The free space path-loss exponent is assumed to be $n = 2$. The total loss along a path is the sum of the free-space path loss and the loss associated with partitions present along the propagation path. A straight line is used to model the insertion loss versus frequency [27]. The fitted insertion transfer functions for different materials and their corresponding parameters for the linear fit are borrowed from [18].

In the narrowband context, the path loss with respect to 1 m free space at a point located at distance d from the reference point is described by the following equation:

$$PL(d) = 20\log_{10}(d) + a \times X_a + b \times X_b \ldots, \tag{10}$$

where a, b, etc., are the numbers of each partition type and X_a, X_b, etc., are their respective attenuation values measured in dB [28]. To extend this concept to UWB communication channels, we introduce the frequency-dependent version of Eq. (10):

$$PL(d,f) = 20\log_{10}(d) + a \times X_a(f) + b \times X_b(f) \ldots, \tag{11}$$

where $X_a(f)$, $X_b(f)$ are the frequency-dependent insertion losses of partitions. Eq. (11) gives the path loss as function of frequency. In order to find the pulse shape and the total power loss we need to find the time-domain equivalent of Eq. (11) by means of inverse Fourier transform over the frequency range of the radiated signal. In doing so, we start with the radiated pulse at a reference distance of 1 m, $p_{\mathrm{rad}}(t)$. In most wideband antennas such as TEM horns, this signal is proportional to the derivative of the input signal fed to the

transmit antenna. Then, we determine the spectrum of the received signal at the location of the receive antenna using the following relationship:

$$P_{\mathrm{rec}}(f) = \frac{P_{\mathrm{rad}}(f)}{[10^{(a\times X_a(f)+b\times X_b(f)\ldots)/20}]d}. \tag{12}$$

It is important to note that the attenuation is applied to the radiated signal rather than to the input signal of the antenna. The transmit antenna alters the spectrum of the input signal as illustrated in Fig. 6. Starting with a Gaussian pulse, the time-domain received signal, $p_{\mathrm{rec}}(t)$, is obtained by inverse Fourier transforming $P_{\mathrm{rec}}(f)$. With the received pulse determined, one is able to assess pulse distortion and the total power loss.

In this example we illustrate how to utilize the material characterization results and apply them to a partition problem. The objective is to find the power loss through a propagation path and to estimate the pulse shape and the frequency distribution of the

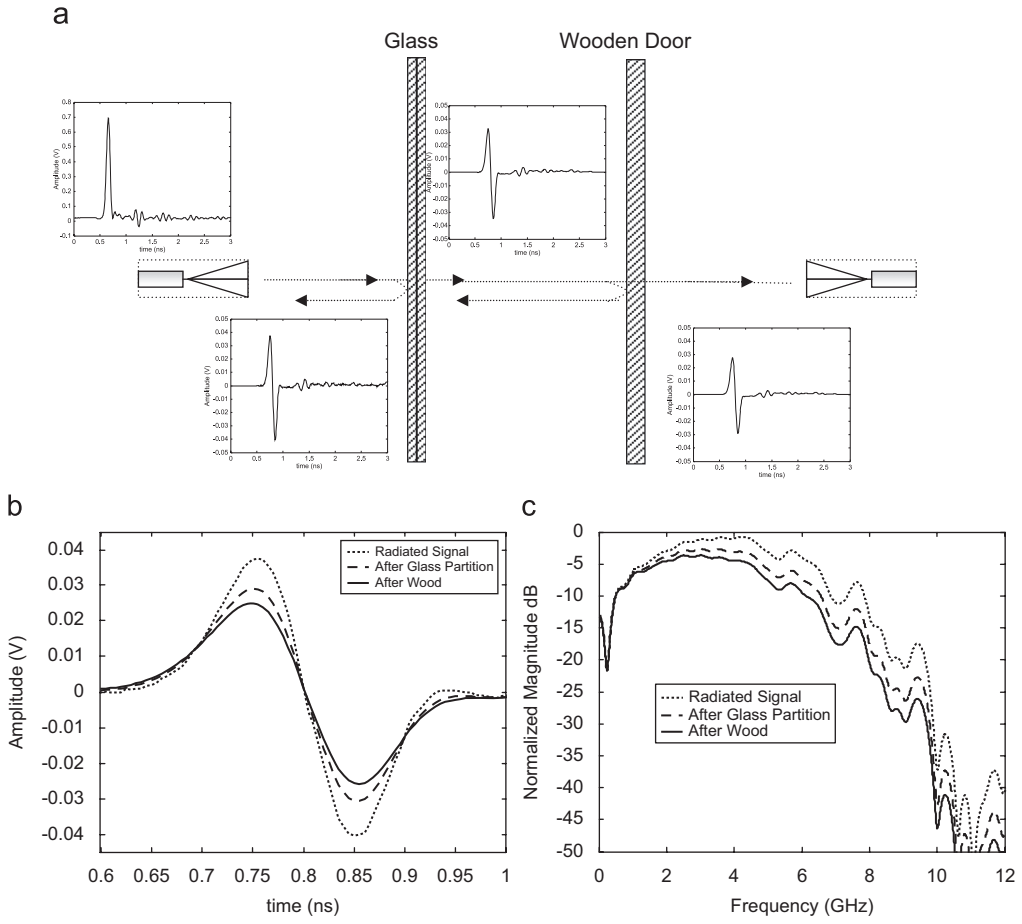

Fig. 6. Illustrative example for UWB partition dependent modeling: (a) illustration of the partitions setup, (b) frequency distribution of the signal at different points, and (c) radiated signal, signal after the glass partition, and the signal after the wooden door.

received signal. Consider a LOS path with two partitions present between two TEM horn antennas as shown in Fig. 6a. The first partition is a double sheet of glass and the second is a wooden door with the same thickness as those characterized in [18]. The input signal to the antenna and that radiated from it are displayed in this figure. These signals were obtained through measurements.

To estimate the signal passed through the glass partition, Fourier transform is used to determine the spectrum of the radiated signal and the frequency-dependent loss is applied to this spectrum. Inverse Fourier transform is then used to obtain the time-domain signal passed through the glass sheets. The same procedure is repeated to estimate the signal passed through the wooden door partition. The loss in the signal power is evident in Fig. 6b. It is also noted that higher frequencies are smoothed out. The change in frequency distributions is more evident in Fig. 6c. At lower frequencies, the spectra of the signals, namely, the signal transmitted through the glass and that transmitted through the wooden door are very close, whereas at higher frequencies the differences are more pronounced. This analysis is helpful in link-budget analysis and understanding of potential interference effects from indoor to outdoor environments.

7. Conclusions

The potential and challenges in UWB through-wall imaging were discussed. Multi-path, obstructions and angle of transmission and reception relative to the antenna are among the significant challenges towards full utilization of capability of UWB imaging systems. For electromagnetic characterization of common walls, measurements techniques in both time domain and frequency domain were reviewed. Single-pass and multi-pass models were discussed to relate the measured data to the electromagnetic properties of walls made of different materials in the UWB frequency range. Both attenuative and dispersive impacts on UWB signal propagation were addressed.

The frequency dependence was incorporated into the narrowband partition-dependent propagation model. The modified model was applied to a representative example to illustrate its applicability. The model is valuable in evaluating the potential for indoor radar as well as communication system applications. It was shown that the signal spectrum and the medium of propagation determine the extent of the UWB radar application. The effect of frequency dependence should be considered in receiver design for optimal reception.

Acknowledgment

Dr. Muqaibel acknowledges King Fahd University of Petroleum and Minerals, KFUPM, for supporting this research.

References

[1] Section 15.503 Definitions, Subpart F, Ultra Wideband Operation of Revision of Part 15 of the Commission's Rules Regarding Ultra-Wideband Transmission, Federal Communications Commission, ET Docket 98-153, April 2002.

[2] R.A. Scholtz, Multiple access with time-hopping impulse modulation, in: MILCOM'93, vol. 2, 1993, pp. 447–450.

[3] R.J. Fontana, S.J. Gunderson, Ultra-wideband precision asset location system, in: Proceedings of IEEE Conference on Ultra Wideband Systems and Technologies, 21–23 May 2002, pp. 147–150.

[4] N.S. Correal, S. Kyperountas, Q. Shi, M. Welborn, An UWB relative location system, in: Proceedings of IEEE Conference on Ultra Wideband Systems and Technologies, 16–19 November 2003, pp. 394–397.
[5] W. Chung, D. Ha, An accurate ultra wideband (UWB) ranging for precision asset location, in: Proceedings of IEEE Conference on Ultra Wideband Systems and Technologies, 16–19 November 2003, pp. 389–393.
[6] A.M. Attiya, A. Bayram, A. Safaai-Jazi, S.M. Riad, UWB applications for through-wall detection, in: IEEE International Symposium: Antennas and Propagation Society, vol. 3, 20–25 June 2004, pp. 3079–3082.
[7] M. Mahfouz, A. Fathy, Y. Yang, E.E. Ali, A. Badawi, See-through-wall imaging using ultra wideband pulse systems, in: Proceedings of the 34th Applied Imagery and Pattern Recognition Workshop, 19–21 October 2005.
[8] M.Y.W. Chia, S.W. Leong, C.K. Sim, K.M. Chan, Through-wall UWB radar operating within FCC's mask for sensing heart beat and breathing rate, in: European Radar Conference, EURAD, 6–7 October 2005, pp. 267–270.
[9] C. Gentile, A. Kik, A Comprehensive Evaluation of Indoor Ranging Using Ultra-Wideband Technology, EURASIP Journal on Wireless Communications and Networking, Vol. 2007, Article ID 86031, 10 pp, 2007, doi:10.1155/2007/86031.
[10] S. Hantscher, A. Reisenzahn, C.G. Diskus, An UWB wall scanner based on a shape estimating SAR algorithm, in: International Microwave Symposium, IEEE-MTT-S, 3–8 June 2007, pp. 1463–1466.
[11] H. Hashemi, The indoor radio propagation channel, Proc. IEEE 81 (1993) 943–968.
[12] Y.P. Zhang, Y. Hwang, Measurements of the characteristics of indoor penetration loss, in: IEEE 44th Vehicular Technology Conference, vol. 3, 1994, pp. 1741–1744.
[13] O. Landron, M.J. Feuerstein, T.S. Rappaport, A comparison of theoretical and empirical reflection coefficients for typical exterior wall surfaces in a mobile radio environment, IEEE Trans. Antennas Propag. 44 (3) (1996) 341–351.
[14] H. Suzuki, A.S. Mohan, Measurement and prediction of high spatial resolution indoor channel characteristic map, IEEE Trans. Veh. Technol. 49 (4) (2000) 1321–1333.
[15] H.L. Bertoni, Radio Propagation for Modern Wireless Systems, Prentice-Hall PTR, New Jersey, 2000, p. 55.
[16] S.N. Kharkovsky, U.C. Hasar, M.F. Akay, C.D. Atis, Measurement and monitoring of microwave reflection and transmission properties of cement based materials for propagation modeling, in: Proceedings of the 53rd Vehicular Technology Conference, vol. 2, 2001, pp. 1202–1206.
[17] I. Cuinas, M.G. Sanchez, Measuring, modeling, and characterization of indoor radio channel at 5.8 GHz, IEEE Trans. Veh. Technol. 50 (2) (2001) 526–535.
[18] A. Muqaibel, A. Safaai-Jazi, A. Attiya, B. Woerner, S.M. Riad, UWB through-the-wall propagation, IEE Proc. Microwave Antennas Propag. 152 (6) (2005) 581–588.
[19] D. Pena, R. Feick, H.D. Hristov, W. Grote, Measurement and modeling of propagation losses in brick and concrete walls for the 900-MHz band, IEEE Trans. Antennas Propag. 51 (1) (2003) 31–39.
[20] O.V. Mazurin, M.V. Streltsina, Handbook of Glass Data, Part A: Silica Glass and Binary Silicate Glasses, Elsevier, New York, 1983.
[21] G.I. Torgivnikov, Dielectric Properties of Wood and Wood-Based Materials, Springer, New York, 1993.
[22] A. Muqaibel, Characterization of UWB communication channels, Ph.D. Dissertation, Virginia Polytechnic Institute and State University, Blacksburg, VA, USA, 2003.
[23] B.P. Donaldson, M. Fattouche, R.W. Donaldson, Characterization of in-building UHF wireless radio communication channels using spectral energy measurements, IEEE Trans. Antennas Propag. 44 (1996) 80–86.
[24] A.H. Muqaibel, A. Safaai-Jazi, A new formulation for characterization of materials based on measured insertion transfer function, IEEE Trans. Microwave Theory Tech. 51 (8) (2003) 1946–1951.
[25] F.J. Aurand, Measurements of transient electromagnetic propagation through concrete and sand, Sandia Report SAND96-2254 UC-706, Sandia National Laboratories, Livermore, CA 94550, 1996.
[26] C.R. Anderson, T.S. Rappaport, K. Bae, A. Verstak, N. Ramakrishnan, W. Tranter, C. Shaffer, L. Watson, In-building wideband multipath characteristics at 2.5 & 60 GHz, in: Proceedings of IEEE 56th Vehicular Technology Conference, vol. 1, 2002, pp. 97–101.

[27] T. Gibson, D. Jenn, Prediction and measurements of wall insertion loss, IEEE Trans. Antennas Propag. 47 (1) (1999) 55–57.
[28] G. Durgin, T.S. Rappaport, H. Xu, Measurements and models for radio path loss and penetration loss in and around homes and trees at 5.85 GHz, IEEE Trans. Commun. 46 (11) (1998) 1484–1496.